Journal of Molecular Liquids 457 (2026) 129798

Contents lists available at ScienceDirect

Journal of Molecular Liquids

journal homepage: www.elsevier.com/locate/molliq

Microwave-assisted synthesis of benzalkonium-based deep eutectic solvents: Physicochemical properties and DFT insights into hydrogen-bonding

Rachel A. Maia [a,b], Carlos V. dos Santos Jr [b,c], Isadora Maria G. Andrade [d], Emelly Suelen F.R. Santos [e], Aleff C. de Castro [e], Malu Maria L. dos Reis [e,f], Elquio E. Oliveira [f], Claudio Gabriel Lima-Junior [e], Elfi Kraka [g], Renaldo T. Moura Jr. [b,g], Dayse N. Moreira [e,*]

[a] Department of Fundamental Chemistry, Federal University of Pernambuco, Recife 50670-901, PE, Brazil
[b] Academic Unit of Cabo de Santo Agostinho, Federal Rural University of Pernambuco, Cabo de Santo Agostinho, 54518-430, PE, Brazil
[c] Department of Chemistry and Physics, Federal University of Paraíba, Campus II, Areia 58397-000, PB, Brazil
[d] Department of Organic Chemistry, Federal University Fluminense, Niterói 24020-005, RJ, Brazil
[e] Laboratory of Medicinal Organic Synthesis of Paraíba (LASOM-PB), Department of Chemistry, Federal University of Paraíba, João Pessoa 58051-900, PB, Brazil
[f] Laboratory of Synthesis and Drug Delivery, State University of Paraíba, João Pessoa 58071-160, PB, Brazil
[g] Computational and Theoretical Chemistry Group (CATCO), Department of Chemistry, Southern Methodist University, Dallas, TX 75275, USA

ARTICLE INFO

Keywords:
Benzalkonium chloride
Intermolecular interactions
Microwave-assisted synthesis
Density functional theory

ABSTRACT

The search for alternative solvent systems has gained increasing attention in organic synthesis due to the need for more sustainable solvents. In this regard, deep eutectic solvents (DES) have emerged as promising alternatives because of their tunable physicochemical properties, simple preparation, and potential alignment with Green Chemistry principles. Furthermore, understanding the structural organization and intermolecular interactions within these systems is essential for rationalizing their physicochemical behavior and guiding the design of new functional solvents. In this study, benzalkonium chloride-based DES were prepared using a microwave-assisted approach by combining benzalkonium chloride as the hydrogen bond acceptor (HBA) with different hydrogen-bond donors (HBDs), namely citric acid, oxalic acid, and glycerol, at equimolar ratios. Rheological characterization was employed to investigate the structural organization and flow properties of the obtained materials. Fourier Transform Infrared Spectroscopy (FTIR) and Density Functional Theory (DFT) calculations revealed the formation of hydrogen-bond interactions between the benzalkonium salt and the hydroxyl groups of the HBDs, confirming the establishment of the supramolecular network responsible for DES formation. Theoretical analyses further demonstrated that the strength and nature of intermolecular interactions vary significantly among the systems, and these differences are directly reflected in their thermal behavior and structural organization. Overall, this study provides a comprehensive structure-property relationship by combining experimental and computational approaches, highlighting the key role of intermolecular interactions in determining the physicochemical properties of DES.

1. Introduction

In recent decades, significant efforts have been made to replace classic organic solvents with sustainable alternatives due to the intrinsic drawbacks of these solvents, including flammability, high volatility, toxicity, and environmental damage [1,2]. This fact boosted the development of nonconventional/nontraditional solvents, such as the deep eutectic solvents (DES) [1,3–5]. Among these systems, DES has garnered increasing attention from the scientific community for its tunable properties, making these mixtures viable alternatives to toxic organic solvents.

DES are formed by a mixture of two or more components in suitable molar ratios, resulting in a eutectic mixture, *i.e.*, one with a melting point lower than that of the individual components [6,7]. DES can be classified into five types, and Type III has the most applications due to its low cost and low ecotoxicity. Generally, these mixtures are prepared

* Corresponding author.
E-mail address: daysenm@gmail.com (D.N. Moreira).

https://doi.org/10.1016/j.molliq.2026.129798
Received 28 April 2026; Received in revised form 9 June 2026; Accepted 9 July 2026
Available online 10 July 2026

from halide salts (*e.g.,* quaternary ammonium salts - Quats) or hydrogen bond acceptors (HBA) with compounds that can donate hydrogen bonds (HBD), such as urea, acids, or amines [2]. The interaction of HBDs with quaternary ammonium salts (HBAs) occurs through charge delocalization between HBD and halide ions, which leads to a decrease in the melting point and forms a DES [8].

One of the most studied HBAs is choline chloride (ChCl - 2-hydroxyethyl-trimethylammonium chloride), a naturally occurring and bifunctional compound that contains both quaternary ammonium and hydroxyl moieties. Despite this structure offering many advantages as a DES former, one limitation concerns the hydroxyl group, particularly when the chosen HBD is a carboxylic acid. The esterification product was recently observed, albeit in small amounts (7% for ChCl:oxalic acid; 19% for CHCl:malic acid), after heating the mixture at 80 °C [9]. Florindo et al. [10] have also reported this behavior when preparing this DES at 100 °C. Among Quats, benzalkonium chloride (BC), a mixture of alkyl, benzyl, and dimethyl ammonium chlorides [$C_6H_5CH_2N(CH_3)_2R$] Cl, with an octyl chain (C_8H_{17}) as the main constituent, does not contain a hydroxyl group in its chain, which minimizes the formation of byproducts. BC belongs to the cationic surfactants with antimicrobial activity against a variety of bacteria, fungi, and yeasts, and is also used in the chemical products industry, including disinfectants, biocides, detergents, anti-electrostatic agents, and phase-transfer catalysts [11,12].

In the case of HBD, citric acid, oxalic acid, and glycerol are among the most attractive hydrogen-bond donors for the preparation of deep eutectic solvents due to their low toxicity, biodegradability, low cost, and renewable origin. These compounds make citric acid-, oxalic acid-, and glycerol-based DES promising green solvents for extraction processes, biomass processing, catalysis, and organic synthesis [13,14].

Usually, DES can be prepared relatively simply [3,12] using various methods [3,12], employing either conventional or non-conventional techniques. The most commonly used method involves heating and stirring the components of the DES, without adding solvent, until a homogeneous liquid is obtained. Other methods for DES preparation include vacuum evaporation, freeze-drying, and grinding. However, the previously mentioned methods have some limitations, including difficulty in scaling up, which significantly limits contact between the starting materials, and difficulty forming hydrogen bonds. In addition, conventional methods require a longer formation time to obtain the solvent due to non-uniform conduction heating [15]. Although these methods have been extensively and effectively employed for DES syntheses, few works have concerned investigating other heating sources [16–18]. In this context, we highlight the use of microwave irradiation as a promising technique to be investigated, as it has demonstrated several advantages, including higher product yields and milder and shorter reaction times [9,19]. The heating process with MW is through the dielectric mechanism, which may involve dipolar polarization and ionic conduction. However, this process depends on the ability of the chemical compounds to absorb microwave energy and turn it into heat, and consequently, results in bulk heating [19]. Thus, the intrinsic polarity and ionic character of HBAs and HBDs are fundamental to the MW dielectric heating response [9].

From a molecular perspective, the structural organization of DES is governed by complex intermolecular interactions, primarily hydrogen bonding, electrostatic forces, and dispersion interactions. Recent studies have combined experimental infrared (IR) spectroscopy with theoretical approaches to identify the main intermolecular interactions in DES, particularly by comparing spectral shifts relative to the pure components, thereby elucidating their structural arrangement [20–22]. These analyses reveal that DES formation leads to significant perturbations in vibrational modes, reflecting strong interactions between HBA and HBD. In particular, the role of the anion (HBA counterion, *e.g.*, Cl^-) present in the DES system is fundamental for understanding its physicochemical properties. In this sense, Density Functional Theory (DFT) calculations have emerged as a powerful tool to describe these interactions at the molecular level. Through optimized geometries, interaction energy calculations, and analysis of electronic properties (such as charge distribution, frontier molecular orbitals, and electrostatic potential maps), DFT provides detailed insights into the strength and nature of HBA-HBD interactions, as well as the role of the anion in stabilizing the supramolecular structure [21].

Considering the growing interest in developing sustainable solvent systems aligned with the principles of Green Chemistry, this work reports the microwave-assisted synthesis of benzalkonium chloride-based deep eutectic solvents (DES) using different hydrogen bond donors (citric acid, oxalic acid, and glycerol). Despite the growing number of studies on DES, investigations of systems derived from benzalkonium salts remain scarce, particularly regarding their rheological behavior. In this context, the present study provides a comprehensive evaluation of the flow properties of these systems, contributing to a better understanding of their macroscopic behavior. Furthermore, computational investigations based on Density Functional Theory (DFT) were employed to elucidate the intermolecular interactions and structural organization within the DES network. Together, these results contribute to expanding the knowledge of benzalkonium-based DES and provide insights that may support the rational design of new functional solvent systems.

2. Experimental

2.1. Chemicals

Citric acid monohydrate (Vetec), oxalic acid dihydrate (Vetec, 99.5–102.5%), benzalkonium chloride (Sigma Aldrich ≥95%), and glycerol (Neon ≥97%) were dried under vacuum before use. All reactants were kept in a desiccator to avoid moisture absorption. The molecular structures of the HBA and HBDs used in the DES synthesis are shown in Fig. 1.

2.2. Preparation of deep eutectic solvents (DES) under conventional heating

The preparation of deep eutectic solvents (DES) was performed similarly to Qin et al. [23] by mixing the quaternary ammonium salt (benzalkonium chloride - BC) and the hydrogen bond donor (oxalic acid - OA, citric acid - CA, or glycerol - G) previously dried, in a 1:1 M ratio. The mixture of components was stirred continuously at 100 °C for 2 h until a homogeneous, viscous liquid was formed. Subsequently, they were placed under vacuum to remove moisture and stored in a desiccator containing anhydrous calcium chloride and silica gel before characterization.

2.3. Preparation of deep eutectic solvents (DES) under microwave irradiation

The preparation of deep eutectic solvents (DES) was performed by mixing the quaternary ammonium salt (benzalkonium chloride – BC) and the hydrogen bond donor (oxalic acid - OA, citric acid - CA, or glycerol - G) previously dried, in a 1:1 M ratio, in a sealed quartz tube (microwave-specific vessel). The mixture was irradiated at 80 °C for 1–2 min, under constant cooling. The ramp time was approximately 1 min. All three synthesized DES remained liquid after about 24 h at room temperature; no further purification steps were needed. Subsequently, they were placed under vacuum to remove moisture and stored in a desiccator containing anhydrous calcium chloride and silica gel before the characterization.

2.4. NMR spectroscopy

^1H and ^{13}C nuclear magnetic resonance (NMR) spectra were recorded on a Bruker Avance II 400 (^1H at 400 MHz and ^{13}C at 100 MHz) at

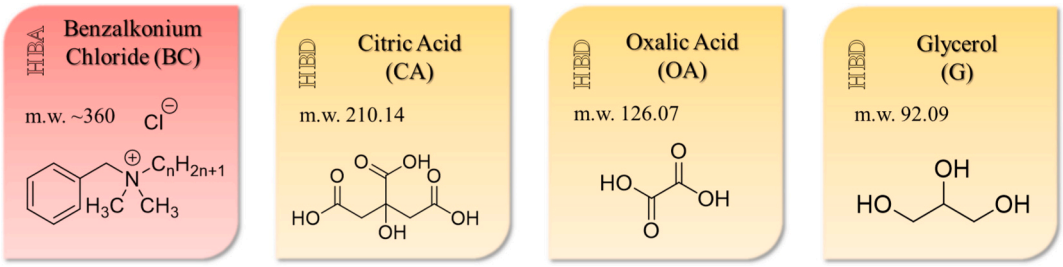

Fig. 1. HBA and HBDs structures used in the benzalkonium-DES synthesis.

room temperature in 5 mm sample tubes in deuterated chloroform/tetramethylsilane ($CDCl_3$/TMS) solutions (digital resolution ±0.01 ppm).

2.5. Attenuated total reflectance-fourier transform infrared spectroscopy analysis (ATR-FTIR)

The infrared spectra of the DES synthesized by the different methods, as well as those of the initial materials, were obtained using an Agilent Cary 630 FTIR spectrometer operated in attenuated total reflectance mode (ATR-FTIR) in the wavenumber region between 4000 and 400 cm^{-1}, with a resolution of 4 cm^{-1}. Each sample was scanned 8 times, and the data obtained was analyzed using the IR resolution software.

2.6. Microwave irradiation (MW)

Reactions requiring microwave irradiation were performed in a microwave reactor model system (Discover CEM benchmate), with temperature monitored by a built-in infrared sensor in simultaneous-cooling mode.

2.7. Thermophysical properties

DSC (Differential Scanning Calorimetry, TA Instrument Model DSC Q20) and TGA (Thermogravimetric Analysis, TA Instruments Model TGA Q50) were used to measure the thermal properties of the prepared eutectic mixtures.

2.7.1. Differential scanning calorimetry (DSC) analysis

DES thermal behavior was performed using sealed aluminum pans, at a rate of 5 °C/min, from −80 °C until the degradation temperature of each mixture, under nitrogen flow (50 mL/min). The amount of sample in each measurement ranged from 10 to 15 mg.

2.7.2. Thermogravimetric analysis (TGA)

Thermal decomposition analyses of the DES synthesized, as well as the starting materials, were performed using Pt pans, at a rate of 10 °C/min, from 25 to 300 °C under nitrogen flow (40 mL/min). The amount of sample in each measurement ranged from 10 to 15 mg.

2.8. Physicochemical characterization

The density was measured at 25 °C by weighing the DES after filling a 1 mL volumetric flask up to the calibrated mark. The density was calculated as follows: $r = m/V$ (where m was the weight (g) of the DES in the volumetric flask and V was the volume of the DES (mL). The refractive index was measured using a digital portable refractometer (Hanna Instruments, model HI96801, 0–85%Brix), calibrated with distilled water (nD = 1.33). The ionic conductivity of pure DES was measured in a Mod. LUCA-150 MC (cell constant K = 1, working range: 0 to 200,000 mS/cm), with a platinum sensor, and equipped with an individual stainless steel temperature sensor. BC-based DES solubility was measured in different solvents (*i.e.*, water, DMSO, acetonitrile, methanol, ethanol, acetone, dichloromethane, ethyl acetate, chloroform, diethyl ether, toluene, benzene, and hexane). The mixtures were added to test tubes, vortexed at 25 °C, and the solubility was determined by observing the separation of the DES and the organic solvent, following a protocol adapted from that described by Shafie et al. [24].

2.9. Rheological measurements

The experiments were performed at 25 ± 0.1 °C using a rheometer MCR302e (Anton Paar, Australia) equipped with a cone-and-plate geometry PP25 (1° cone angle, 25 mm of diameter), based on [25]. Prior to testing, the samples were allowed to equilibrate on the geometry for 5 min to ensure thermal and structural stability. The apparent viscosity and shear stress were recorded as functions of shear rate for each DES individually. All the samples were analyzed in triplicate.

2.10. Computational section

2.10.1. Theoretical methods of hydrogen bond analysis

There are many approaches to exploring hydrogen bonds in molecular systems. We selected four theoretical models to investigate our DES systems: the Noncovalent Interaction (NCI) method [26], Quantum Theory of Atoms in Molecules (QTAIM) [27,28], local [29–31], and the Overlap Model (OP/TOP) [32,33]. The first approach enables qualitative characterization of intermolecular interactions by analyzing the reduced density gradient (RDG) in regions of low electronic density. The $sign(\lambda_2)\rho$ parameter, as defined in [26], is used to classify NCI regions as strong attractive, van der Waals, or strong repulsive interactions. QTAIM analysis is based on a topological exploration of the electronic density of the molecule, identifying critical points where the gradient of the electron density ($\Delta\rho$) is zero. The nature of intermolecular interactions can be investigated *via* descriptors calculated at bond critical points (BCPs), typically localized between interacting atoms. Following the Cremer-Kraka [34] criterion, more negative values of the total energy density (H_{BCP}) at the BCP can be used to identify the covalent character of an intermolecular interaction.

Local vibrational mode theory offers an ingenious way to access the information encoded in the vibrational analysis of molecular systems. Konkoli and Cremer [29] introduced a theoretical formalism that allows the decomposition of normal vibrational modes into local vibrational modes, yielding local force constants that can be directly associated with bond strengths or with angle and dihedral displacements. Thus, this theory has been applied to study the strength of hydrogen bonds in a wide variety of molecular systems [35–38]. Finally, the OP/TOP approach performs a decomposition of molecular density into two-center contributions associated with a pair of bonded atoms, referred to as the overlap density (ρ_{OP}) [33]. This portion of the electron density has been used as a quantitative index of the orbital overlap. The model was initially developed to describe the chemical environment of lanthanide ions in complexes [39,40] and was later reformulated [41,42] to study chemical bonds and intermolecular interactions in molecular systems. As demonstrated in previous studies [43,44], overlap density descriptors are useful tools for quantifying orbital overlap

interactions present in hydrogen bonds.

2.10.2. Computational procedure

We performed a supramolecular analysis of the BC:CA, BC:OA, and BC:G systems by constructing clusters of six DES units to account for cooperative intermolecular effects. The choice of six DES units was based on a trade-off between experimental data agreement and computational resource requirements. Full geometry optimizations were carried out at the extended tight-binding level, as implemented in ORCA 6 [45], using the GFN2-xTB [46] method, followed by harmonic vibrational frequency calculations to confirm the nature of the stationary points and to obtain infrared vibrational spectra. All optimized structures were characterized as true minima by the absence of imaginary frequencies (*supplementary material*). NCI analysis was subsequently applied using the NCIPLOT4 [47] software to identify and characterize intermolecular interactions within the clusters. The analysis was performed using the promolecular density approximation [48], which is suitable for large systems.

From the optimized clusters, intermolecular bond distances of the OH•••Cl and CH•••Cl interactions were extracted for each DES unit, and average values were computed. The unit presenting the smallest deviation from these average geometric parameters was selected as the representative structure for subsequent electronic analyses. Single-point calculations were then performed on the selected fragment at the ωB97X-D3/def2-TZVP [49,50], level of theory, as implemented in ORCA 6 [45], employing tight SCF convergence criteria and the RIJCOSX [51] approximation. The OH•••Cl and CH•••Cl intermolecular interactions were analyzed using the QTAIM, LVM, and OP/TOP models. Topological descriptors were calculated from the wavefunction using Multiwfn [52] while OP/TOP and LVM descriptors were computed using ChemBOS [53] and LModeA [54] respectively.

3. Results and discussion

3.1. Preparation of DES

The three benzalkonium-based DES were prepared using two methods: conventional heating (oil bath) and microwave irradiation. The first method, based on conventional heating, involved mixing equal amounts of HBA and HBD (Fig. 1), followed by continuous stirring at 100 °C for 2 h until a homogeneous and viscous liquid was formed. All eutectic mixtures remained liquid without any precipitates at ambient temperature, even after a month in a desiccator.

The microwave-assisted method has also been shown to be a valuable alternative to investigate, as it can reduce reaction time, an important principle of green chemistry, particularly due to the DES components, which are effective microwave absorbers. Thus, we decided to examine DES synthesis under microwave irradiation, considering that intrinsic polarity and ionic behavior are the two main solvent properties responsible for the MW dielectric heating [9]. For the DES based on citric acid [BC:CA], 2 min were required for the mixture to become a liquid, whereas the DES containing glycerol and oxalic acid as HBDs required only 1 min of irradiation at 80 °C with constant stirring. These results corroborate the previous findings of Gonzalez et al. [55], which also reported a decrease in preparation time for sugar/organic acid DES systems. On the other hand, evaluating the DES thermal stability at higher temperatures is mandatory to verify the starting materials and the DES integrity under microwave irradiation. Thus, the temperature was increased to 100 °C, during 1 min of irradiation; however, a dark solution was obtained, indicating DES decomposition. These results are consistent with the observed data reported by González-Rivera et al. [9].

The appearance of the eutectic solvents based on organic acids is very viscous liquids, at room temperature, since their formation occurs due to strong hydrogen bonding of the precursors, along with intermolecular interactions involving Van der Waals and electrostatic forces. Indeed, determining physicochemical parameters is crucial for understanding their flow behavior, especially when used as solvents in organic synthesis protocols (Table 1).

3.2. Physicochemical properties

3.2.1. Density

Density plays a fundamental role in the design and selection of deep eutectic solvents (DES), as it offers valuable insights into the internal interactions and structural organization of these complex mixtures. In this study, the density of benzalkonium-based DES ranges from 1.01 to 1.22 g.mL^{-1} (Table 2), which is higher than that of its individual components. This behavior is due to the formation of extensive hydrogen bonding networks, which reduce the average free volume between molecules. This behavior is often explained by the hole theory, where the mixing of hydrogen bond donors (HBDs) and acceptors (HBAs) leads to a more compact molecular arrangement, resulting in a denser liquid phase [56]. Thus, the greater the number of hydroxyl groups in the HBD, the more hydrogen bonding can occur, thereby reducing the molar free volume of the DES system and resulting in higher DES density [57,58]. In addition, several factors, including the nature and molar ratio of components, temperature, and the presence of water, also influence the density of a DES [24].

3.2.2. Refractive index

The refractive index (RI), nD, is a crucial physical property of materials, such as solvents, and consists of the measurement of the propagation of light through a given sample. This measurement can provide valuable insights into the purity of the material. In this study, all the obtained DES exhibited higher values than water (1.33), with nD ranging from 1.489 to 1.502. The obtained data can be compared with those reported by Bakht et al. (2016) for DES systems with a BC core and urea as the HBD, which ranged from 1.4466 to 1.457 [21]. The refractive index is also related to the electronic polarizability of the medium [7]. Hence, the DES with a BC has a higher refractive index because the aromatic ring is highly polarizable.

3.2.3. Ionic conductivity

Ionic conductivity refers to the ability of a material to transport ions, effectively measuring how readily it allows the flow of electric current *via* the movement of charged species. DES systems can be used as a component of electrolytes; therefore, ionic conductivity is essential for applications in electrochemistry and industrial development [59] The conductivities of the BC-based DES values varied between 1.45 mS.cm^{-1} and 700.60 mS.cm^{-1} (Table 2). DES based on dicarboxylic acids (BC:OA) exhibited higher conductivity than those based on other simple carboxylic acids, as previously observed by Abbott et al. [7]. On the other hand, low ionic conductivity (generally less than 2 mS.cm^{-1}) is expected for highly viscous eutectic solvents, as we observed for BC:*CA*. This result is in accordance with the case of ChCl:CA (1:1), where the conductivity was recorded to be 1.82 mS.cm^{-1} at room temperature [60].

3.2.4. Solubility

Another essential property of the DES characterization is its miscibility with organic solvents and water, which contributes to its application in several fields, especially in organic synthesis. The unique

Table 1
– Acronym, molecular ratio, molecular weight, and apparency of prepared DES.

Acronym	Molar ratio	Mol wt. (g/mol)	Apparency
[BC:CA]	1:1	596.25	Transparent viscous liquid
[BC:OA]	1:1	445.06	Transparent viscous liquid
[BC:G]	1:1	447.12	Transparent liquid

BC: benzalkonium chloride; CA: citric acid; OA: oxalic acid; G: glycerol.

Table 2
– Density (r), refractive index (nD), and electrical conductivity (κ) data of synthesized DES, obtained at 25 °C.

Entry	DES	r (g.mL^{-1})	nD	κ (mS.cm^{-1})
1	[BC:CA]	1.22	1.489	1.45
2	[BC:OA]	1.07	1.500	700.60
3	[BC:G]	1.01	1.502	109.60

Water density as reference value: 0.998 (g.mL^{-1}) at 25 °C.

feature of DES is the existence of both cationic and anionic components, as well as non-ionic species, which enhances its solubility in a wide range of solvents. Thus, for these tests, we selected a series of solvents with varying polarities (nonpolar, polar, and intermediate), as presented in Table 3.

All synthesized DES exhibited good miscibility with polar organic solvents and consequently had higher dielectric constants. This behavior can be attributed to the dielectric constant, which is directly related to the solvent's ability to stabilize and separate charges, a property strongly influenced by the electronic organization and polarizability of the molecules [61]. In contrast, for the organic solvents, with lower dielectric constants, typically nonpolar or of low polarity, the DES demonstrated low or no solubility, indicating limited compatibility with less polar media (Table 3). The results indicate that these DES have a hydrophilic character due to the high polarity of the HBDs, citric and oxalic acids, and hygroscopic behavior due to benzalkonium chloride [3].

3.3. Thermal stability of benzalkonium-based DES

3.3.1. Thermogravimetric analysis (TGA)

Understanding the thermal profile of DES is fundamental, as its use is similar to that of classical solvents and requires heating for various applications, including biocatalysis, organic reactions, biomass processing, natural products extractions, and others. However, unlike molecular solvents, which are usually single-use, DES can be reused multiple times without degradation. Thus, the study of thermal degradation provides essential information on thermal stability and the maximum operating temperatures for use in chemical and physical processes without weight loss, ensuring that heat transfer does not compromise functionality [62].

The thermal stability of the DES was investigated by TGA and differential thermogravimetric (DTG) analysis up to 300 °C, and the thermogram curves are shown in Fig. 2. The analysis of the thermogram curves was based on three parameters: (a) the initial decomposition temperature, at which DES exhibits a significant weight loss of 5–10%; (b) the onset temperature of sample thermal degradation (T_{onset}), which determines the operative temperature range in which the samples can be used without decomposing, and (c) the T_d (temperature of maximum degradation rate), identified as the temperature corresponding to the peak maximum in the derivative curve (DTG) [63] (Table 4). (See Table 5.)

The data obtained demonstrate that the observed degradation reflects an initial loss of varying amounts of water that was absorbed during DES handling or sample preparation, due to the strong hygroscopic character of the components. Deep eutectic solvents (DES) remain in the liquid state without undergoing any degradation up to their initial decomposition temperature [67]. These properties are intrinsic to the material and can be observed even at elevated temperatures. DES [BC:G] and [BC:OA] exhibited a single-stage thermal decomposition at 198 °C and 199 °C, respectively. On the other hand, in DES [BC:CA], the thermal decomposition pattern was observed to occur in two successive stages at 201 °C and 282 °C. This behavior can be explained by the presence of clusters with slightly different thermal stability, highlighting the complex nature of these compounds [68].

The deep eutectic solvent synthesized with oxalic acid as the hydrogen-bond donor (HBD) exhibited the lowest thermal stability among the DES studied. This result was expected, considering that the thermal stability of DES is directly related to the number and strength of possible intermolecular interactions. In this context, citric acid, due to its greater capacity to form hydrogen bonds, resulted in the DES with the highest observed thermal stability.

Thermal degradation of deep eutectic solvents (DES) has been widely reported and is closely related to the nature of the hydrogen bond donor (HBD) and the HBA:HBD molar ratio, as these parameters determine the strength and distribution of intermolecular hydrogen-bonding interactions within the system [68]. The temperatures of the mass loss for pure HBD decreased in the following order: CA > G > OA, in agreement with the decomposition temperature of pure HBDs (Table 4). They are shifted to lower temperatures when HBDs are in DES, maintaining the same relative order. All DES investigated in this work have the same HBA (BC). The thermal decomposition of pure BC showed a single, sharp mass loss of about 96% in the temperature of 171 °C, with a $T_d = 218$ °C, which resulted in a slightly lower temperature when BC was in the DES systems.

3.3.2. Differential scanning calorimetry

DSC analysis allows us to determine the endothermic and exothermic thermal events of the DES and identify the glass transition temperatures (T_g) of the synthesized solvents. The results show that all DES presented glass transition temperatures (T_g) ranging from −40.22 to −67.6 °C, indicating the presence of an amorphous region with a high degree of disorder that may hinder solvent solubilization.

For DES [BC:CA], only T_g was identified; therefore, it does not exhibit crystallinity events and possesses high mechanical and thermal strength. The others, in addition to presenting T_g, also had melting temperatures (T_m), indicating that they are semicrystalline materials. For the DES [BC:OA], two distinct melting transitions (T_m) were observed, occurring at −11.01 °C and 45.02 °C, respectively. On the other hand, the DES [BC:G] exhibited a single T_m at −16.66 °C. These results confirm that deep eutectic solvents are formed by the combination of two components through self-association *via* hydrogen bonding. This interaction typically results in a new mixture with a freezing point significantly lower than that of its individual components.

Table 3 - DES
miscibility in different solvents.

	Solvent	Dielectric constant	BC: CA	BC: OA	BC: G
Polar	*Water*	78.54	m	m	m
	DMSO	47.00	m	m	m
	Acetonitrile	36.64	m	m	m
	Methanol	32.60	m	m	m
	Ethanol	24.60	m	m	m
	Acetone	21.01	m	m	m
Intermediate	*Dichloromethane*	9.08	m	m	m
	Ethyl Acetate	6.02	m	m	m
	Chloroform	4.81	m	m	m
	Diethyl Ether	4.26	m	m	m
Nonpolar	*Toluene*	2.38	nm	nm	nm
	Benzene	2.28	pm	pm	pm
	Hexane	1.89	nm	nm	nm

m = miscible; nm = non miscible; pm = partial miscible.

3.4. Rheology

The rheological characterization of the synthesized benzalkonium-based deep eutectic solvents (DES) was performed to elucidate the relationship between their macromolecular flow properties and the underlying hydrogen-bonding network, as depicted in Fig. 3.

The apparent viscosity measurements, performed at 25 °C, revealed a distinct order of viscosity among the DES systems: [BC:CA] > [BC:OA] > [BC:G] (39.31, 37.94, 0.725 Pa, respectively), which is in high agreement with the experimental density data (1.22 > 1.07 > 1.01 g

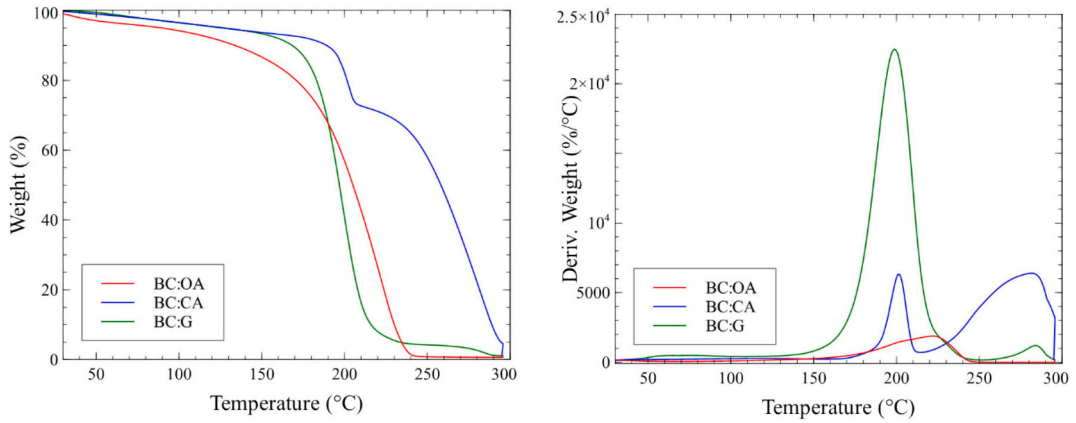

Fig. 2. TGA and DTG analysis for the three DES systems: [BC:CA] (blue line), [BC:OA] (red line), and [BC:G] (green line). (For interpretation of the references to colour in this figure legend, the reader is referred to the web version of this article.)

Table 4
- Thermal properties obtained from TGA data for the DES under study, namely, degradation temperature (T_d).

	HBA		HBD		DES	
	$T_{(5\%)}/T_{onset}$ (°C)	T_d (°C)	$T_{(5\%)}/T_{onset}$ (°C)	T_d (°C)	$T_{(5\%)}/T_{onset}$ (°C)	T_d (°C)
BC:CA	111/171	218	73.7/201	249	109.5	201/282
BC:OA	111/171	218	90/164	113/203	109.3	199
BC:G	111/171	218	96/176	244	71.6	198

Table 5
Thermal properties obtained from DSC data for the DES under study, namely, the temperature of glass transition (T_g), freezing and melt temperature ($T_{freezing}$ and T_{melt}) obtained in the last DSC cycle.

DES	T_g / °C	$T_{freezing}$ / °C	T_{melt} / °C	Ref
OA	–	34	190	[7,64]
CA	–	69	149	[7,64]
Gly	–	–	17.8	[64,65]
BC	–	-1	–	[66]
BC:OA	−40.22	−25.12/−5.31	−11.01/45.02	This work
BC:CA	−67.60	–	–	This work
BC:G	−45.55	−24.88	−16.66	This work

cm^{-3}) and the enhanced thermal stability observed for the citric acid-based DES. This indicates that the viscosity is highly dependent on the nature of the constituting components, specifically the hydrogen bond donor (HBD) [69,70].

The [BC:G] system exhibited a predominantly Newtonian behavior within the investigated shear rate range (1–100 s^{-1}). In this regime, the viscosity remained independent of the shear rate, suggesting a relatively fluid supramolecular arrangement with reduced internal friction. Conversely, the organic acid-based systems [BC:CA] and [BC:OA] exhibited pronounced pseudoplastic (shear-thinning) behavior. For these systems, a significant reduction in apparent viscosity was observed as the shear rate increased. This phenomenon is typically attributed to the progressive disruption or alignment of the extensive intermolecular interaction networks under mechanical stress [67,71].

In fact, the possibility of controlling the properties of a DES for a given application type depends directly on its constituents.

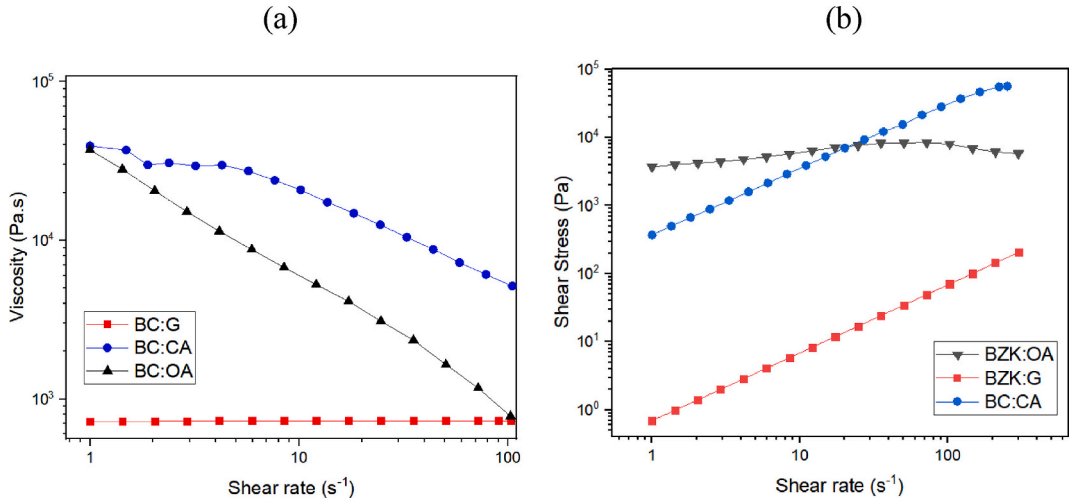

Fig. 3. (a) log-log representation of the apparent viscosity *vs* shear rate of the DES systems and (b) log-log representation of the shear stress variation as a function of applied shear rate for the studied DES systems.

3.5. Infrared spectroscopy

FTIR analysis is a widely used technique for identifying the characteristic absorption bands associated with functional groups and chemical bonds present in synthesized benzalkonium-based DES. Moreover, it provides valuable evidence of the hydrogen-bonding interactions established between the components, which are essential for deep eutectic solvent formation. For the DES BC:OA, *e.g.*, the broad ν(O—H) stretching band shifted from 3477 to 3422 cm^{-1} in the pure components to 3426 cm^{-1} in the DES and became noticeably broader, indicating the establishment of stronger intermolecular hydrogen bonds. In contrast, the aliphatic C—H stretching bands of BC showed only minor shifts (2922/2854 to 2926/2855 cm^{-1}), suggesting that the hydrophobic domains remained largely unaffected. More significant changes were observed in the carbonyl region, where the bands at 1682 cm^{-1} (OA) and 1648 cm^{-1} (BC) were shifted to 1746 and 1736 cm^{-1}, respectively,

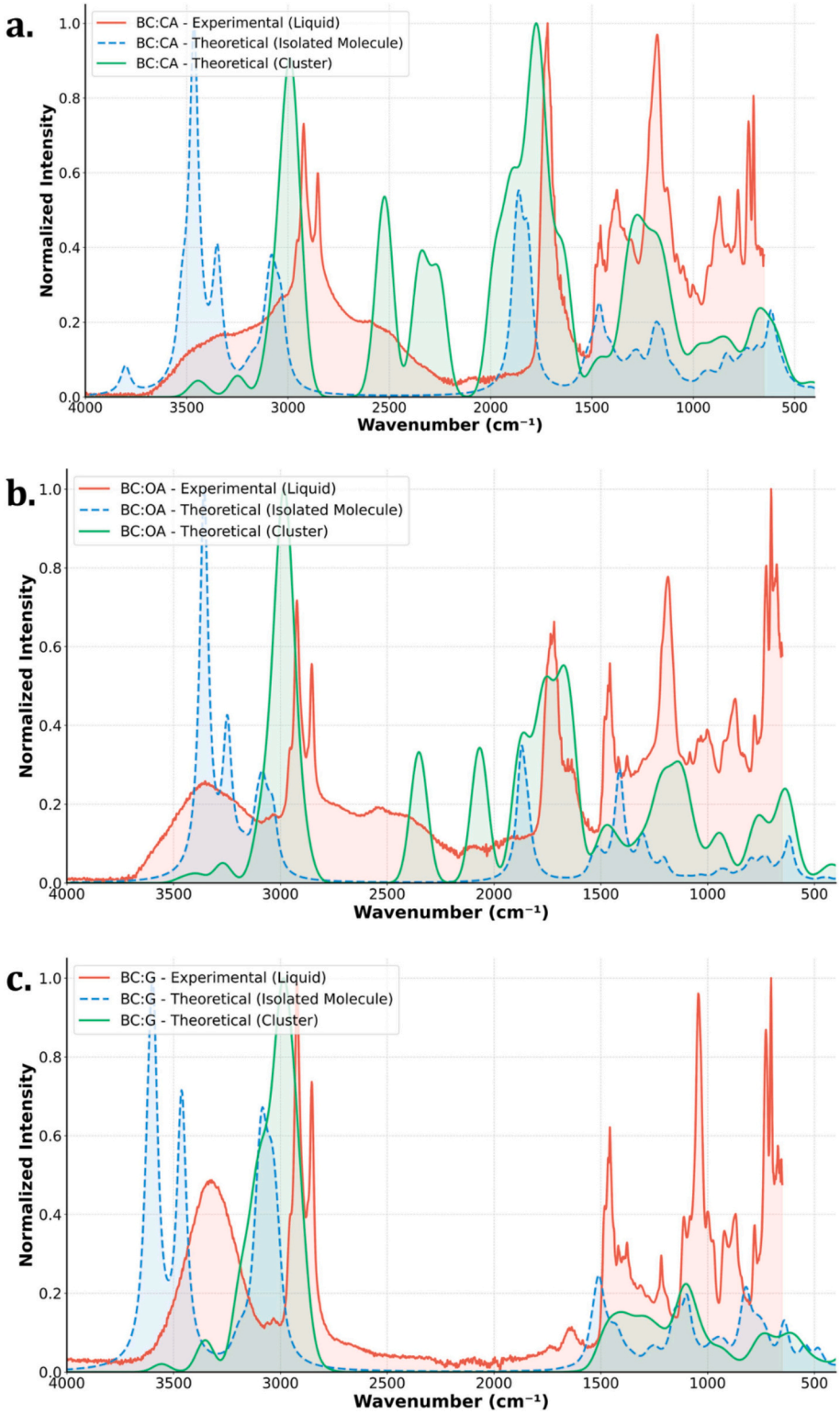

Fig. 4. Experimental and theoretical infrared spectra.

in the DES, reflecting changes in the electronic environment of the carbonyl groups due to intermolecular interactions. Additionally, the ν(C—O) and ν(C–O–C) stretching bands underwent noticeable shifts, with the BC band at 1220 cm^{-1} moving to approximately 1200 cm^{-1} and the OA bands at 1234 and 1131 cm^{-1} reorganizing into new absorptions at 1265 and 1200 cm^{-1}. These spectral changes confirm the involvement of oxygen-containing functional groups in the hydrogen-bond network responsible for DES formation (See supplementary material ***S16-S18***).

After the IR experimental characterization, the obtained data were compared with the theoretical IR data. Fig. 4 depicts the experimental and theoretical infrared spectra (for the isolated molecule and a cluster of six molecules) of [BC:CA], [BC:OA], and [BC:G].

Angular frequency measurements *vs* stretching of hydroxyl and carboxyl groups are present in the range 3600–2600 cm^{-1}. Citric and Oxalic acids have more vibrations in this range since they are di- and tricarboxylic acids [72]. Broad and intense bands in this region, attributed to the ν(O—H) stretching vibrations associated with hydrogen bond formation, are characteristic features of DES systems.

The shape and width of these bands may also be influenced by the presence of moisture, an effect detectable in the experimental FTIR spectra. In the theoretical spectra of the isolated monomers, the individual O—H stretching contributions appear as more defined bands, such as 3348 and 3463 cm^{-1} for [BC:CA], 3248 and 3357 cm^{-1} for [BC:OA], and 3462 and 3618 cm^{-1} for [BC:G]. In contrast, the cluster models display broader absorption ranges, for example, from 3257 to 2518 cm^{-1} in [BC:CA], reflecting the collective effect of intermolecular interactions. This broadening indicates the formation of an extended hydrogen-bond network and reproduces more closely the behavior observed in the experimental spectra.

The carbonyl stretching bands ν(C=O), present in [BC:CA] and [BC:OA], are experimentally observed in 1719 and 1719 cm^{-1}, respectively. In the theoretical monomer calculations, these bands appear at higher wavenumbers 1859 cm^{-1} in [BC:CA] and 1843 cm^{-1} in [BC:OA], due to the absence of stabilizing intermolecular interactions. The C–O–C stretching vibrations appear experimentally at 1177 cm^{-1} [BC:CA], 1185 cm^{-1} [BC:OA], and 1042 cm^{-1} [BC:G], while theoretical values are slightly shifted 1138–1203 cm^{-1}. The vibrations associated with methylene and methyl groups, CH_2/CH_3, appear in the experimental spectra at 2922 and 2852 cm^{-1} across all systems, whereas theoretical calculations predict slightly broader ranges ≈ of 2930 to 3110 cm^{-1}, reflecting the absence of medium effects in the computational model.

Aromatic ring vibrations of the benzalkonium cation are experimentally observed between 702 and 727 cm^{-1} and theoretically predicted in the range of 641–734 cm^{-1}. Overall, good qualitative agreement is observed between the experimental and theoretical spectra. While many studies [73–76] have calculated infrared spectra for a single isolated DES unit, herein, we evaluated both isolated and cluster models, demonstrating that the theoretical infrared spectra are improved when considering more than one interacting DES molecule. The main vibrational assignments and corresponding wavenumbers are summarized in the *supplementary material*.

3.5.1. Hydrogen bond analysis

As previously mentioned, a single isolated molecule does not account for all intermolecular interactions in the DES, and it is crucial to perform a general analysis before any local analysis. Therefore, we employed the NCI method to identify the weak interactions in the studied clusters ([BC:CA], [BC:OA], and [BC:G]), and the results are illustrated in Fig. 5.

Figs. 5a–c show green isosurfaces at the contact regions between the carbon chains of the DES molecules, corresponding to van der Waals interactions [79]. Also, blue isosurfaces at the OH···Cl contacts and red isosurfaces within the aromatic rings of the BC molecule indicate strong attractive hydrogen bonds and strong repulsive interactions, respectively [79].

Figs. 5d–f depict the RDG *vs* $sign(\lambda_2)\rho$ plots for the studied systems, showing a broader van der Waals region for [BC:CA] (Fig. 4d) than for [BC:OA] and [BC:G]. This result corroborates experimental observations showing that van der Waals interactions within [BC:CA] directly affect its density and viscosity. The relationship between viscosity and van der Waals interactions in DES is well-established in the literature [73,80,81] Additionally, the RDG plots of [BC:CA] (Fig. 5d) and [BC:OA] (Fig. 5e) exhibit attractive interaction peaks at −0.06 a.u. In contrast, the [BC:G] system (Fig. 5f) exhibits blue peaks at −0.05 a.u., indicating that its hydrogen bonds are weaker than those in the [BC:CA] and [BC:OA] systems.

The hydrogen bonds within the clusters were also investigated using the LVM theory [82]. Fig. 6 displays the stretching force constants of two key hydrogen bonds in the DES: OH• • •Cl and CH• • •Cl interactions.

Fig. 6 demonstrates that the OH• • •Cl interactions in the [BC:CA] cluster are stronger than the other two clusters, showing values of k_a

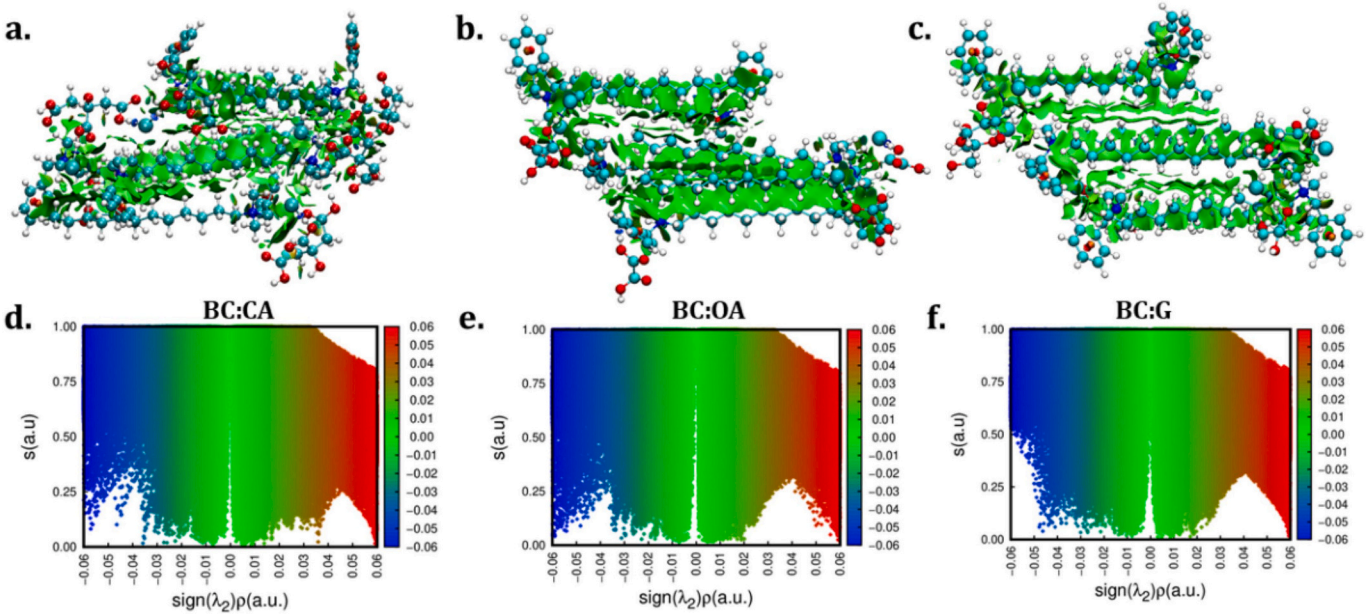

Fig. 5. NCI isosurfaces for the [BC:CA] (a), [BC:OA] (b), and [BC:G] (c) clusters with a cutoff = 0.3, created using the VMD program [77]. In addition, the RDG *vs.* $sign(\lambda_2)\rho$ plot for the [BC:CA] (d), [BC:OA] (e), and [BC:G] (f) clusters, generated using the NCIWEB [78].

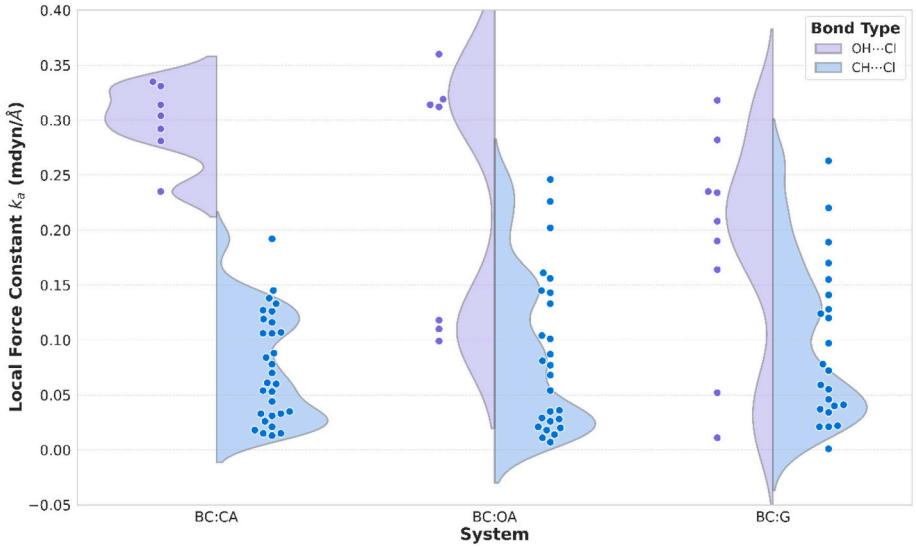

Fig. 6. Local force constants (k_a) for OH• • •Cl (purple) and CH• • •Cl (blue) interactions in the [BC:CA] (a), [BC:OA] (b), and [BC:G] (c) clusters. (For interpretation of the references to colour in this figure legend, the reader is referred to the web version of this article.)

near 0.30 mdyn•Å^{-1}. This result agrees with experimental findings that [BC:CA] is more thermally stable than [BC:OA] and [BC:G] because of its hydrogen bond strength. Additionally, the [BC:OA] (Fig. 6b) and [BC:G] (Fig. 6c) present some CH• • •Cl interactions with force constants higher than 0.20 mdyn•Å^{-1}, while all CH• • •Cl interactions in [BC:CA] are lower than 0.20 mdyn•Å^{-1}. These findings highlight the importance of cluster analysis, which enables the investigation of all possible contacts that the DES molecule can form with neighboring molecules, thereby explaining experimental properties directly associated with hydrogen bond strength. A similar approach has been employed to study the bimodality effect on water clusters [83].

Although physicochemical properties of DES are better reproduced using the cluster model, there is no reason to completely avoid the isolated molecule model. When analyzing only local interactions, such as the OH···Cl hydrogen bond, modeling the system with a single molecule allows us to improve the level of theory used to describe the interaction. Thus, we selected a single DES molecule from each cluster and performed geometry optimization, vibrational frequency, and hydrogen bond analyses at the ωB97X-D/def2TZVP level of theory, using QTAIM and OP/TOP theories. Fig. 7 illustrates the overlap maps and descriptors derived from the QTAIM (H_{BCP}) and OP/TOP (J_{OP}^{intra}) methods. The complete set of descriptors is available in Table S2 of the *supporting information*.

The overlap maps demonstrate that the OH···Cl hydrogen bonds in [BC:OA] and [BC:CA] exhibit a higher concentration of overlap density than those in [BC:G]. Furthermore, lower values of energy density at the bond critical point (H_{BCP}) and high values of intra-overlap Coulomb repulsion (J_{OP}^{intra}) indicate that the OH···Cl interaction in [BC:CA] (Fig. 7a) is the less electrostatic and electron-rich. However, the [BC:G] system features CH···Cl interactions with the less electrostatic character (lower H_{BCP}) and electron richness (higher J_{OP}^{intra}). These findings are consistent with the LVM (Fig. 6) and the NCI analysis (Fig. 5), confirming that [BC:CA] exhibits the strongest, less electrostatic, and most electron-rich OH···Cl interactions.

Finally, we can observe that Density Functional Theory (DFT) calculations support these rheological findings. Reduced Density Gradient (RDG) analysis revealed that the [BC:CA] cluster exhibits a significantly larger region of van der Waals interactions than the other systems. This extensive network of weak cooperative contacts contributes to a higher cohesive energy density, manifesting as increased viscosity and density. Furthermore, Local Vibrational Mode (LVM) analysis quantified the strength of the OH···Cl$^-$ interactions. The [BC:CA] system exhibited the highest force constants, indicating robust and highly directional hydrogen bonds that stabilize the supramolecular structure. Interestingly, the [BC:G] system showed CH···Cl$^-$ interactions with a less electrostatic character. These results indicate that the high viscosity of [BC:CA] arises from a synergistic effect between strong, localized hydrogen bonds and an extensive van der Waals interaction surface, whereas the fluidity of [BC:G] is governed by a molecular organization that favors local ionic stability over global structural rigidity. The synergy between OP/TOP, QTAIM, LVM, and NBO descriptors was recently demonstrated for covalent and non-covalent interactions in different contexts [43,44]. For hydrogen bonds, a direct comparison of overlap density descriptors with NBO populations and stabilization energies [43,44] reveals OP/TOP as a complementary, reliable methodology to inspect the nature of chemical bonds.

4. Conclusions

In this study, we report the microwave-assisted synthesis of three benzalkonium-based deep eutectic solvents (DES). The synthesized DES were obtained as highly viscous liquids at room temperature and exhibited high solubility in various solvent classes. In addition to the well-established advantages of DES as safer and more sustainable solvents since they are typically composed of low-toxicity or non-toxic components, the microwave-assisted synthetic approach employed here contributes to improved energy efficiency and reduced processing time.

The combined analysis of TGA, DSC, and miscibility results demonstrates that benzalkonium chloride-based DES exhibits physicochemical properties strongly influenced by the nature of the hydrogen bond donor. Thermogravimetric curves revealed that the BC:CA system exhibits higher thermal stability, followed by BC:OA and BC:G, reflecting distinct decomposition profiles attributable to differences in intermolecular interactions. These findings are consistent with the DSC data, which showed significantly low glass transition temperatures, confirming the formation of eutectic systems with high structural disorder and strong interactions between components.

The physicochemical behavior of these systems was well correlated with the density functional theory (DFT) calculations and experimental viscosity measurements from rheology. This combined theoretical-experimental approach provided a deeper understanding of how intermolecular interactions influence macroscopic properties. Differences in interaction patterns, particularly involving OH···Cl and CH···Cl contacts,

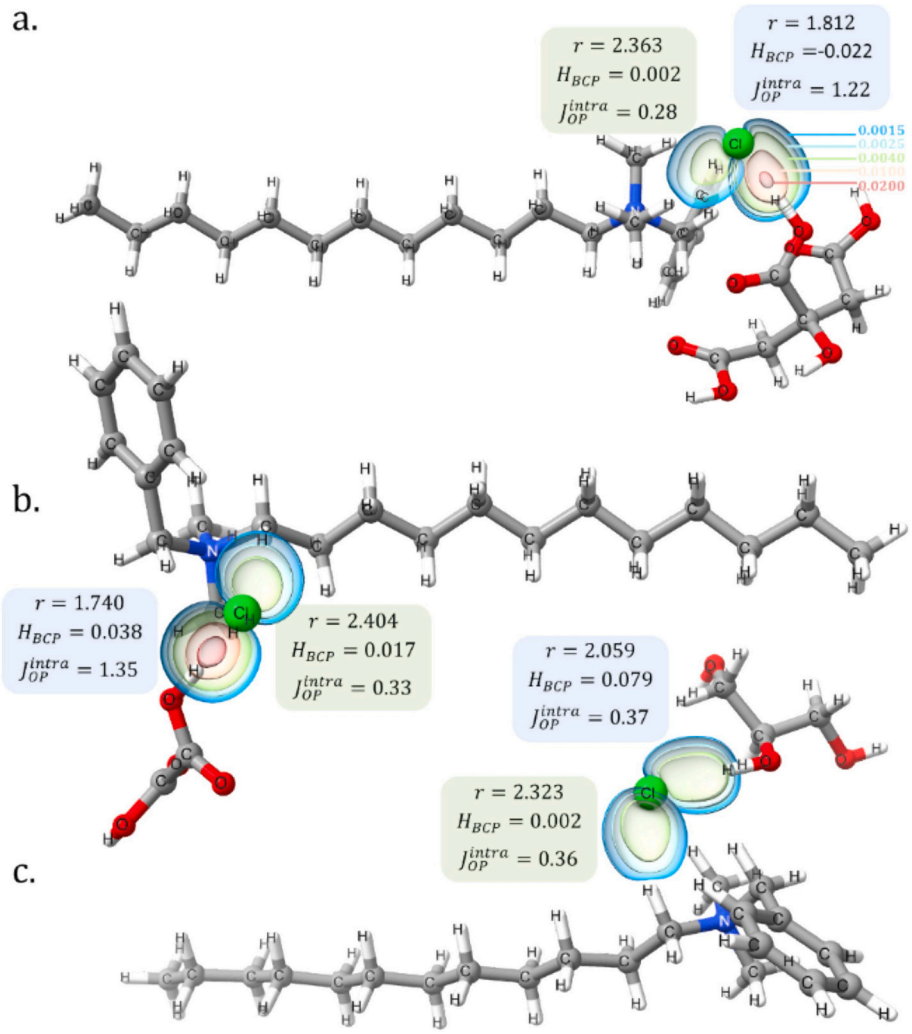

Fig. 7. Overlap density maps of OH• • •Cl and CH• • •Cl intermolecular interactions calculated for one DES molecule extracted from each cluster: (a) [BC:CA], (b) [BC:OA], and (c) [BC:G]. Isovalues between 0.0015 and 0.0200 e/a_0^3 are represented by a red-green-blue colour scheme, illustrated in (a). Calculations were performed at the ωB97X-D3/def2TZVP level of theory, and the maps were generated with ChimeraX [85–87] program. The distance r (in Å), intra-overlap Coulomb repulsion J_{OP}^{intra} (in E_h), and energy density at the BCP H_{BCP} (in E_h/a_0^3) of each interaction are also highlighted. (For interpretation of the references to colour in this figure legend, the reader is referred to the web version of this article.)

were shown to directly affect structural arrangement and fluidity, emphasizing how subtle variations in hydrogen-bond donors can modulate the overall behavior of DES. These findings contribute to a deeper understanding of structure–property relationships and support the rational design of DES for advanced applications in green chemistry and solvent engineering.

CRediT authorship contribution statement

Rachel A. Maia: Writing – review & editing, Writing – original draft, Methodology, Investigation, Formal analysis, Data curation, Conceptualization. **Carlos V. dos Santos:** Writing – review & editing, Writing – original draft, Methodology, Investigation, Formal analysis, Data curation, Conceptualization. **Isadora Maria G. Andrade:** Writing – review & editing, Writing – original draft, Methodology, Investigation, Formal analysis, Data curation, Conceptualization. **Emelly Suelen F.R. Santos:** Writing – review & editing, Writing – original draft, Methodology, Formal analysis, Data curation, Conceptualization. **Aleff C. de Castro:** Writing – original draft, Methodology, Formal analysis, Data curation, Conceptualization. **Malu Maria L. dos Reis:** Writing – original draft, Methodology, Investigation, Formal analysis, Data curation, Conceptualization. **Elquio E. Oliveira:** Writing – review & editing, Writing – original draft, Methodology, Investigation, Formal analysis, Data curation, Conceptualization. **Claudio Gabriel Lima-Junior:** Writing – original draft, Methodology, Investigation, Conceptualization. **Elfi Kraka:** Writing – review & editing, Writing – original draft, Software, Methodology, Formal analysis, Data curation, Conceptualization. **Renaldo T. Moura:** Writing – review & editing, Writing – original draft, Software, Investigation, Funding acquisition, Formal analysis, Data curation, Conceptualization. **Dayse N. Moreira:** Writing – review & editing, Writing – original draft, Software, Investigation, Funding acquisition, Formal analysis, Data curation, Conceptualization

Declaration of competing interest

The authors declare the following financial interests/personal relationships which may be considered as potential competing interests: Dayse das Neves Moreira reports financial support was provided by Paraiba Federal University. Dayse das Neves Moreira reports a relationship with National Council for Scientific and Technological Development that includes: employment and funding grants. If there are other authors, they declare that they have no known competing financial interests or personal relationships that could have appeared to influence the work reported in this paper.

Acknowledgments

The authors acknowledge financial support and fellowships from the Brazilian agency, the National Council for Scientific and Technological Development (CNPq, Grant no. 404236/2021-9, 406483/2023-0, 310988/2023-3, and 404742/2024-6). This work was supported by CNPq (Brazilian Agency) through INCT-LumiNanoTec (grant 408501/2024-3). The authors also thank the CM-ACQuimBio at Paraiba State University for analytical support.

Data availability

No data was used for the research described in the article.

References

[1] C.J. Clarke, W.C. Tu, O. Levers, A. Bröhl, J.P. Hallett, Green and sustainable solvents in chemical processes, Chem. Rev. 118 (2018) 747–800, https://doi.org/10.1021/acs.chemrev.7b00571.
[2] A. Sanjeeta, J. Singh, Kavirajwar, Dynamic properties and diverse applications of deep eutectic solvents, J. Ionic Liq. 5 (2025) 100135, https://doi.org/10.1016/j.jil.2025.100135.
[3] D.S. Wagare, S.E. Shirsath, M. Shaikh, P. Netankar, Sustainable solvents in chemical synthesis: a review, Environ. Chem. Lett. 19 (2021) 3263–3282, https://doi.org/10.1007/s10311-020-01176-6.
[4] T.R. Sekharan, O. Katari, S.N. Ruhina Rahman, D.M. Pawde, A. Goswami, R. M. Chandira, T. Shunmugaperumal, Neoteric solvents for the pharmaceutical industry: an update, Drug Discov. Today 26 (2021) 1702–1711, https://doi.org/10.1016/j.drudis.2021.03.005.
[5] V. Hessel, N.N. Tran, M.R. Asrami, Q.D. Tran, N. Van Duc Long, M. Escribà-Gelonch, J.O. Tejada, S. Linke, K. Sundmacher, Sustainability of green solvents – review and perspective, Green Chem. 24 (2022) 410–437, https://doi.org/10.1039/D1GC03662A.
[6] A.P. Abbott, G. Capper, D.L. Davies, R.K. Rasheed, V. Tambyrajah, Novel solvent properties of choline chloride/urea mixtures, Chem. Commun. (2003) 70–71, https://doi.org/10.1039/b210714g.
[7] A.P. Abbott, D. Boothby, G. Capper, D.L. Davies, R.K. Rasheed, Deep eutectic solvents formed between choline chloride and carboxylic acids: versatile alternatives to ionic liquids, J. Am. Chem. Soc. 126 (2004) 9142–9147, https://doi.org/10.1021/ja048266j.
[8] A.P. Abbott, R.C. Harris, K.S. Ryder, C. D'Agostino, L.F. Gladden, M.D. Mantle, Glycerol eutectics as sustainable solvent systems, Green Chem. 13 (2011) 82–90, https://doi.org/10.1039/C0GC00395F.
[9] J. González-Rivera, E. Husanu, A. Mero, C. Ferrari, C. Duce, M.R. Tinè, F. D'Andrea, C.S. Pomelli, L. Guazzelli, Insights into microwave heating response and thermal decomposition behavior of deep eutectic solvents, J. Mol. Liq. 300 (2020) 112357, https://doi.org/10.1016/j.molliq.2019.112357.
[10] C. Florindo, A.J.S. McIntosh, T. Welton, L.C. Branco, I.M. Marrucho, A closer look into deep eutectic solvents: exploring intermolecular interactions using solvatochromic probes, Phys. Chem. Chem. Phys. 20 (2017) 206–213, https://doi.org/10.1039/c7cp06471c.
[11] B. Grillitsch, O. Gans, N. Kreuzinger, S. Scharf, M. Uhl, M. Fuerhacker, Environmental risk assessment for quaternary ammonium compounds: a case study from Austria, Water Sci. Technol. (2006) 111–118, https://doi.org/10.2166/wst.2006.840.
[12] A. Fazlara, M. Ekhtelat, The disinfectant effects of Benzalkonium chloride on some important foodborne pathogens, J. Agric. Environ. Sci 12 (2012) 23–29.
[13] O. Długosz, M. Banach, Green methods for obtaining deep eutectic solvents (DES), J. Clean. Prod. 434 (2024) 139914, https://doi.org/10.1016/j.jclepro.2023.139914.
[14] F.J.V. Gomez, M. Espino, M.A. Fernández, M.F. Silva, A greener approach to prepare natural deep eutectic solvents, ChemistrySelect 3 (2018) 6122–6125, https://doi.org/10.1002/slct.201800713.
[15] A.P.R. Santana, J.A. Mora-Vargas, T.G.S. Guimarães, C.D.B. Amaral, A. Oliveira, M. H. Gonzalez, Sustainable synthesis of natural deep eutectic solvents (NADES) by different methods, J. Mol. Liq. 293 (2019), https://doi.org/10.1016/j.molliq.2019.111452.
[16] F.S. Costa, L.S. Moreira, A.M. Silva, R.J. Silva, M.P. dos Santos, E.G.P. da Silva, M. T. Grassi, M.H. Gonzalez, C.D.B. Amaral, Natural deep eutectic solvent-based microwave-assisted extraction in the medicinal herb sample preparation and elemental determination by ICP OES, J. Food Compos. Anal. 109 (2022), https://doi.org/10.1016/j.jfca.2022.104510.
[17] G. Chatel, R.S. Varma, Ultrasound and microwave irradiation: contributions of alternative physicochemical activation methods to green chemistry, Green Chem. 21 (2019) 6043–6050, https://doi.org/10.1039/c9gc02534k.
[18] S.L. Perkins, P. Painter, C.M. Colina, Experimental and computational studies of choline chloride-based deep eutectic solvents, J. Chem. Eng. Data 59 (2014) 3652–3662, https://doi.org/10.1021/je500520h.
[19] A.N. El-hoshoudy, F.S. Soliman, E.M. Mansour, T. Zaki, S.M. Desouky, Experimental and theoretical investigation of quaternary ammonium- based deep eutectic solvent for secondary water fl ooding, J. Mol. Liq. 294 (2019) 111621, https://doi.org/10.1016/j.molliq.2019.111621.
[20] P.S. Singh, Th.G. Devi, Spectroscopic and computational methods in the characterization of deep eutectic solvent, Gallic acid, and glycerol, Spectrosc. Lett. 57 (2024) 580–607, https://doi.org/10.1080/00387010.2024.2387804.
[21] H. Qin, X. Hu, J. Wang, H. Cheng, L. Chen, Z. Qi, Overview of acidic deep eutectic solvents on synthesis, properties and applications, green, Energy Environ. 5 (2020) 8–21, https://doi.org/10.1016/j.gee.2019.03.002.
[22] M.H. Shafie, R. Yusof, C.Y. Gan, Synthesis of citric acid monohydrate-choline chloride based deep eutectic solvents (DES) and characterization of their physicochemical properties, J. Mol. Liq. 288 (2019), https://doi.org/10.1016/j.molliq.2019.111081.
[23] R. Sulthan, A. Reghunadhan, R. Sreenath, B. Shankar, S. Sambhudevan, Preparation, physicochemical analyses, and comparative evaluation studies of deep eutectic solvents (DES) from non-conventional precursor materials applied as catalytic curing agents for epoxy resin, J. Mol. Liq. 404 (2024) 124940, https://doi.org/10.1016/j.molliq.2024.124940.
[24] E.R. Johnson, S. Keinan, P. Mori-Sánchez, J. Contreras-García, A.J. Cohen, W. Yang, Revealing noncovalent interactions, J. Am. Chem. Soc. 132 (2010) 6498–6506, https://doi.org/10.1021/ja100936w.
[25] R.F.W. Bader, Atoms in molecules, Acc. Chem. Res. 18 (1985) 9–15, https://doi.org/10.1021/ar00109a003.
[26] R.F.W. Bader, A quantum theory of molecular structure and its applications, Chem. Rev. 91 (1991) 893–928, https://doi.org/10.1021/cr00005a013.
[27] Z. Konkoli, D. Cremer, A new way of analyzing vibrational spectra. I. Derivation of adiabatic internal modes, Int. J. Quantum Chem. 67 (1998) 1–9, https://doi.org/10.1002/(SICI)1097-461X(1998)67:1<1::AID-QUA1>3.0.CO;2-Z.
[28] E. Kraka, W. Zou, Y. Tao, Decoding chemical information from vibrational spectroscopy data: local vibrational mode theory, WIREs Computat. Mol. Sci. 10 (2020), https://doi.org/10.1002/wcms.1480.
[29] E. Kraka, M. Quintano, H.W. La Force, J.J. Antonio, M. Freindorf, The local vibrational mode theory and its place in the vibrational spectroscopy arena, J. Phys. Chem. A 126 (2022) 8781–8798, https://doi.org/10.1021/acs.jpca.2c05962.
[30] R.T. Moura, A.N. Carneiro Neto, O.L. Malta, R.L. Longo, Overlap properties of chemical bonds in generic systems including unusual bonding situations, J. Mol. Model. 26 (2020) 301, https://doi.org/10.1007/s00894-020-04535-w.
[31] C.V. Santos-Jr, E. Kraka, R.T. Moura, Chemical bond overlap descriptors from multiconfiguration wavefunctions, J. Comput. Chem. 46 (2025), https://doi.org/10.1002/jcc.27534.
[32] D. Cremer, E. Kraka, Chemical bonds without bonding Electron density — does the difference Electron-density analysis suffice for a description of the chemical bond? Angew. Chem. Int. Ed. Eng. 23 (1984) 627–628, https://doi.org/10.1002/anie.198406271.
[33] A. Madushanka, R.T. Moura, N. Verma, E. Kraka, Quantum mechanical assessment of protein–ligand hydrogen bond strength patterns: insights from semiempirical tight-binding and local vibrational mode theory, Int. J. Mol. Sci. 24 (2023) 6311, https://doi.org/10.3390/ijms24076311.
[34] M. Quintano, A.A.A. Delgado, R.T. Moura Jr., M. Freindorf, E. Kraka, Local mode analysis of characteristic vibrational coupling in nucleobases and Watson–Crick base pairs of DNA, Electronic Structure 4 (2022) 044005, https://doi.org/10.1088/2516-1075/acaa7a.
[35] J.J. Antonio, E. Kraka, Noncovalent π interactions in mutated Aquomet-myoglobin proteins: a QM/MM and local vibrational mode study, Biochemistry 62 (2023) 2325–2337, https://doi.org/10.1021/acs.biochem.3c00192.
[36] M. Quintano, A. Madushanka, C.V. Santos, F.C. Machado, E. Kraka, R.L. Longo, R. T. Moura, Investigating the bimodality of liquid water via chemical bond descriptors and k-means clustering analysis, J. Mol. Liq. 446 (2026) 129306, https://doi.org/10.1016/j.molliq.2026.129306.
[37] O.L. Malta, H.J. Batista, L.D. Carlos, Overlap polarizability of a chemical bond: a scale of covalency and application to lanthanide compounds, Chem. Phys. 282 (2002) 21–30, https://doi.org/10.1016/S0301-0104(02)00631-6.
[38] L.D. Carlos, O.L. Malta, R.Q. Albuquerque, A covalent fraction model for lanthanide compounds, Chem. Phys. Lett. 415 (2005) 238–242, https://doi.org/10.1016/j.cplett.2005.09.001.
[39] R.T. Moura, A.N. Carneiro Neto, O.L. Malta, R.L. Longo, Overlap properties of chemical bonds in generic systems including unusual bonding situations, J. Mol. Model. 26 (2020), https://doi.org/10.1007/s00894-020-04535-w.
[40] C.V. Santos-Jr, E. Kraka, R.T. Moura, Chemical bond overlap descriptors from multiconfiguration wavefunctions, J. Comput. Chem. 46 (2025), https://doi.org/10.1002/jcc.27534.
[41] R.A. Santos, C.V. Santos, E.C. Aguiar, A.N. Carneiro Neto, R.T. Moura, Orbital interactions in hydrogen bonds: a perspective from the chemical bond overlap model, J. Comput. Chem. 46 (2025), https://doi.org/10.1002/jcc.70166.
[42] M. Quintano, A. Madushanka, C.V. Santos, F.C. Machado, E. Kraka, R.L. Longo, R. T. Moura, Investigating the bimodality of liquid water via chemical bond descriptors and k-means clustering analysis, J. Mol. Liq. 446 (2026) 129306, https://doi.org/10.1016/j.molliq.2026.129306.
[43] F. Neese, The ORCA program system, WIREs Comput. Mol. Sci. 2 (2012) 73–78, https://doi.org/10.1002/wcms.81.
[44] C. Bannwarth, S. Ehlert, S. Grimme, GFN2-xTB - an accurate and broadly parametrized self-consistent tight-binding quantum chemical method with multipole electrostatics and density-dependent dispersion contributions, J. Chem. Theory Comput. 15 (2019) 1652–1671, https://doi.org/10.1021/acs.jctc.8b01176.
[45] J. Contreras-García, E.R. Johnson, S. Keinan, R. Chaudret, J.-P. Piquemal, D. N. Beratan, W. Yang, NCIPLOT: a program for plotting noncovalent interaction

regions, J. Chem. Theory Comput. 7 (2011) 625–632, https://doi.org/10.1021/ct100641a.
[46] E.K. Wieduwilt, R.A. Boto, G. Macetti, R. Laplaza, J. Contreras-García, A. Genoni, Extracting quantitative information at quantum mechanical level from noncovalent interaction index analyses, J. Chem. Theory Comput. 19 (2023) 1063–1079, https://doi.org/10.1021/acs.jctc.2c01092.
[47] J. Da Chai, M. Head-Gordon, Long-range corrected hybrid density functionals with damped atom-atom dispersion corrections, Phys. Chem. Chem. Phys. 10 (2008) 6615–6620, https://doi.org/10.1039/b810189b.
[48] F. Weigend, R. Ahlrichs, Balanced basis sets of split valence, triple zeta valence and quadruple zeta valence quality for H to Rn: design and assessment of accuracy, Phys. Chem. Chem. Phys. (2005) 3297–3305, https://doi.org/10.1039/b508541a.
[49] F. Neese, F. Wennmohs, A. Hansen, U. Becker, Efficient, approximate and parallel Hartree-Fock and hybrid DFT calculations. A "chain-of-spheres" algorithm for the Hartree-Fock exchange, Chem. Phys. 356 (2009) 98–109, https://doi.org/10.1016/j.chemphys.2008.10.036.
[50] T. Lu, F. Chen, Multiwfn: a multifunctional wavefunction analyzer, J. Comput. Chem. 33 (2012) 580–592, https://doi.org/10.1002/jcc.22885.
[51] C.V. Santos-Jr, E.M. Lima, R.T. Moura, Numerical integration of overlap electron densities: parallelization strategies for a good load balancing using OpenMP, Comput. Theor. Chem. 1206 (2021), https://doi.org/10.1016/j.comptc.2021.113457.
[52] R.M.Jr., C.V.S.Jr., M.Q.F.B.M.F.D.C.E.K., W. Zou, LModeA2025, 2025.
[53] J. González-Rivera, E. Husanu, A. Mero, C. Ferrari, C. Duce, M.R. Tinè, F. D'Andrea, C.S. Pomelli, L. Guazzelli, Insights into microwave heating response and thermal decomposition behavior of deep eutectic solvents, J. Mol. Liq. 300 (2020), https://doi.org/10.1016/j.molliq.2019.112357.
[54] A.P. Abbott, R.C. Harris, K.S. Ryder, Application of hole theory to define ionic liquids by their transport properties, J. Phys. Chem. B 111 (2007) 4910–4913, https://doi.org/10.1021/jp0671998.
[55] P.G. Yap, Y. Wang, C.Y. Gan, Microwave-assisted preparation of an acidic deep eutectic solvent: green analysis, characterization and application, ChemistrySelect 9 (2024), https://doi.org/10.1002/slct.202400836.
[56] D. Reuter, C. Binder, P. Lunkenheimer, A. Loidl, Ionic conductivity of deep eutectic solvents: the role of orientational dynamics and glassy freezing, Phys. Chem. Chem. Phys. 21 (2019) 6801–6809, https://doi.org/10.1039/c9cp00742c.
[57] T. Jurić, D. Uka, B.B. Holló, B. Jović, B. Kordić, B.M. Popović, Comprehensive physicochemical evaluation of choline chloride-based natural deep eutectic solvents, J. Mol. Liq. 343 (2021), https://doi.org/10.1016/j.molliq.2021.116968.
[58] N. Mqoni, I. Bahadur, S. Singh, X. Meng, A. Ragauskas, Deep eutectic solvents for pretreatment of lignocellulose biomass: physical properties, solubility mechanisms, and their interactions, Chem. Rev. (2026), https://doi.org/10.1021/acs.chemrev.5c00597.
[59] R. Cabezas, F. Olea, E. Zurob, K. Jaramillo, C. Araya-Lopez, M. Ayala, E. Quijada-Maldonado, C. Parra, F. Valdebenito, L. Azocar, Analysis of microwave-assisted heating of deep eutectic solvent: thermal and COSMO-RS study, J. Mol. Liq. 433 (2025) 127775, https://doi.org/10.1016/j.molliq.2025.127775.
[60] M. Carolina Gipiela Corrêa Dias, F. Oliveira Farias, R. Cazelato Gaioto, E. Kaspchak, M. Conceição da Costa, L. Igarashi-Mafra, M.R. Mafra, Thermophysical characterization of deep eutectic solvents composed by D-sorbitol, xylitol or D(+)xylose as hydrogen bond donors, J. Mol. Liq. 354 (2022), https://doi.org/10.1016/j.molliq.2022.118801.
[61] A.K. Jangir, P. Sethy, G. Verma, P. Bahadur, K. Kuperkar, An inclusive thermophysical and rheology portrayal of deep eutectic solvents (DES) for metal oxides dissolution enhancement, J. Mol. Liq. 332 (2021), https://doi.org/10.1016/j.molliq.2021.115909.
[62] J. González-Rivera, C. Pelosi, E. Pulidori, C. Duce, M.R. Tiné, G. Ciancaleoni, L. Bernazzani, Guidelines for a correct evaluation of deep eutectic solvents thermal stability, Curr. Res. Green Sustainable Chem. 5 (2022) 100333, https://doi.org/10.1016/j.crgsc.2022.100333.
[63] H. Zhao, DNA stability in ionic liquids and deep eutectic solvents, J. Chem. Technol. Biotechnol. 90 (2015) 19–25, https://doi.org/10.1002/jctb.4511.
[64] H. Wang, S. Liu, Y. Zhao, J. Wang, Z. Yu, Insights into the hydrogen bond interactions in deep eutectic solvents composed of choline chloride and polyols, ACS Sustain. Chem. Eng. 7 (2019) 7760–7767, https://doi.org/10.1021/acssuschemeng.8b06676.
[65] D. Yang, S. Zhang, X. guang Sun, D. en Jiang, S. Dai, Deep eutectic solvents formed by quaternary ammonium salts and aprotic organic compound succinonitrile, J. Mol. Liq. 274 (2019) 414–417, https://doi.org/10.1016/j.molliq.2018.10.150.
[66] H.K.S. Souza, N. Mateus, V. De Freitas, M.P. Gonçalves, L. Cruz, Chemical/color stability and rheological properties of cyanidin-3-glucoside in deep eutectic solvents as a gateway to design task-specific bioactive compounds, ACS Sustain. Chem. Eng. 8 (2020) 16184–16196, https://doi.org/10.1021/acssuschemeng.0c04839.
[67] E.L. Smith, A.P. Abbott, K.S. Ryder, Deep eutectic solvents (DES) and their applications, Chem. Rev. 114 (2014) 11060–11082, https://doi.org/10.1021/cr300162p.
[68] M.A. Bakht, M.J. Ansari, Y. Riadi, N. Ajmal, M.J. Ahsan, M.S. Yar, Physicochemical characterization of benzalkonium chloride and urea based deep eutectic solvent (DES): a novel catalyst for the efficient synthesis of isoxazolines under ultrasonic irradiation, J. Mol. Liq. 224 (2016) 1249–1255, https://doi.org/10.1016/j.molliq.2016.10.105.
[69] S. Dhibar, S. Babu, A. Mohan, G.K. Chandra, S. Bhattacharjee, K. Karmakar, P. Karmakar, S.K. Mehebub Rahaman, P. Predeep, B. Saha, A novel citric acid facilitated supramolecular zinc(II)-metallogel: toward semiconducting device applications, J. Mol. Liq. 375 (2023) 121348, https://doi.org/10.1016/j.molliq.2023.121348.
[70] A.N. El-hoshoudy, F.S. Soliman, E.M. Mansour, T. Zaki, S.M. Desouky, Experimental and theoretical investigation of quaternary ammonium-based deep eutectic solvent for secondary water flooding, J. Mol. Liq. 294 (2019) 111621, https://doi.org/10.1016/j.molliq.2019.111621.
[71] O. Alioui, W. Sobhi, M. Tiecco, I.M. Alnashef, A. Attoui, A. Boudechicha, K. Kumar Yadav, A.M. Fallatah, N. Elboughdiri, B.-H. Jeon, Y. Benguerba, Theoretical and experimental evidence for the use of natural deep eutectic solvents to increase the solubility and extractability of curcumin, J. Mol. Liq. 359 (2022) 119149, https://doi.org/10.1016/j.molliq.2022.119149.
[72] J. Zhang, J. Yin, Y. Zhang, T. Zhu, H. Ran, W. Jiang, H. Li, H. Li, M. Zhang, Insights into the formation mechanism of aliphatic acid-choline chloride deep eutectic solvents by theoretical and experimental research, J. Mol. Liq. 367 (2022) 120342, https://doi.org/10.1016/j.molliq.2022.120342.
[73] Th.G. Devi, Th.J. Devi, P. Suraj Singh, L. Willingson, Vibrational and molecular properties of curcumin-natural deep eutectic solvent mixture using experimental and theoretical methods, J. Mol. Liq. 397 (2024) 124055, https://doi.org/10.1016/j.molliq.2024.124055.
[74] W. Humphrey, A. Dalke, K. Schulten, VMD: Visual molecular dynamics, J. Mol. Graph. 14 (1996) 33–38, https://doi.org/10.1016/0263-7855(96)00018-5.
[75] J. Contreras-García, E.R. Johnson, S. Keinan, R. Chaudret, J.-P. Piquemal, D. N. Beratan, W. Yang, NCIPLOT: a program for plotting noncovalent interaction regions, J. Chem. Theory Comput. 7 (2011) 625–632, https://doi.org/10.1021/ct100641a.
[76] E.R. Johnson, S. Keinan, P. Mori-Sánchez, J. Contreras-García, A.J. Cohen, W. Yang, Revealing noncovalent interactions, J. Am. Chem. Soc. 132 (2010) 6498–6506, https://doi.org/10.1021/ja100936w.
[77] Q. Zhang, K. De Oliveira Vigier, S. Royer, F. Jérôme, Deep eutectic solvents: syntheses, properties and applications, Chem. Soc. Rev. 41 (2012) 7108, https://doi.org/10.1039/c2cs35178a.
[78] J. Lai, L. Qu, X. Li, Y. Yang, L. Shen, A green and recyclable ternary deep eutectic solvent for extracting flavonol glycoside from Ginkgo leaves: mechanism insights based on molecular level, J. Mol. Liq. 406 (2024) 125053, https://doi.org/10.1016/j.molliq.2024.125053.
[79] E. Kraka, W. Zou, Y. Tao, Decoding chemical information from vibrational spectroscopy data: local vibrational mode theory, WIREs Comput. Mol. Sci. 10 (2020), https://doi.org/10.1002/wcms.1480.
[80] M. Quintano, A. Madushanka, C.V. Santos, F.C. Machado, E. Kraka, R.L. Longo, R. T. Moura, Investigating the bimodality of liquid water via chemical bond descriptors and k-means clustering analysis, J. Mol. Liq. 446 (2026) 129306, https://doi.org/10.1016/j.molliq.2026.129306.
[81] A.J. Schaefer, V.M. Ingman, S.E. Wheeler, SEQCROW: a ChimeraX bundle to facilitate quantum chemical applications to complex molecular systems, J. Comput. Chem. 42 (2021) 1750–1754, https://doi.org/10.1002/jcc.26700.
[82] E.F. Pettersen, T.D. Goddard, C.C. Huang, E.C. Meng, G.S. Couch, T.I. Croll, J. H. Morris, T.E. Ferrin, UCSF ChimeraX: structure visualization for researchers, educators, and developers, Protein Sci. 30 (2021) 70–82, https://doi.org/10.1002/pro.3943.
[83] E.C. Meng, T.D. Goddard, E.F. Pettersen, G.S. Couch, Z.J. Pearson, J.H. Morris, T. E. Ferrin, UCSF ChimeraX: tools for structure building and analysis, Protein Sci. 32 (2023), https://doi.org/10.1002/pro.4792.